



Chapter 8

Optical Correlation: Experiment

Introduction

In this chapter an in depth evaluation of the 16×16 SLM as an optical correlator is performed¹. The relatively low space-bandwidth product of the 16×16 device requires that considerable attention be devoted to the choice of filter algorithm used. Consequently, after an introduction to phase binarisation algorithms in the first section, section two looks at practical filter design and evaluates several novel algorithms devised in this project. Experimental results are compared with those from simulations in section three and the algorithms used are analysed in detail in section four. Section five reviews the results of this chapter.

1 Phase Binarisation Algorithms

The most common approach to computer simulation of optical correlation, as published, is to represent the input object on a 128×128 array, for example, and Fourier Transform this to find the spectrum which is written on an array of identical dimensions. For the binary phase-only matched filters, the phase of the complex number representing the spectrum is conjugated and the binarisation algorithm under evaluation is used to binarise the phase of each spectral data point to either zero or π radians. The amplitude of each point on the filter is set to unity. This procedure is usually applied point by point to make a filter which is used to multiply the original spectrum and obtain the auto-correlation in the image plane.

There are very few publications dealing with the details of filter calculation for use on actual SLMs where the information from several spectral data pixels is required to be combined in some way to produce a single binary phase value for each mirror. Of note, Flannery et al have performed a most extensive study into the application of binary phase-only correlation to machine vision [45]. Experimental work was performed with the 48×48 magneto-optic SLM, described in chapter four, and computer simulations using a 128×128 data array. To match the size of SLM transmissive element with the scale of the FFT, a 3×3 sub-array was averaged to produce a single complex number, the phase of which was used as input to a phase binarisation algorithm, actually that of Horner et al (see following subsection). The filter calculation process of *this* project combines several published phase binarisation algorithms to form a new binarisation procedure applicable to pixellated spatial filters. Briefly, the algorithms used in this project shall now be described.

1.1 Commonly Used Algorithms

Binary phase-only filters are calculated from their continuous filter counterparts by using a binarisation algorithm. If the continuous phase filter $H(\nu)$ (where the discussion relates to a general spatial frequency ν) is of form

$$H(\nu) = e^{-i \Phi(\nu)} \tag{1}$$

where $\Phi(\nu)$ is the phase of the target object Fourier Transform, then

$$H_B(v) = \pm 1 \quad (2)$$

represents the binarised phase-only version of $H(v)$. If the phase of $H(v)$ is plotted on an Argand diagram, one must decide where to divide the plane such that phases on either side are mapped to the poles of either 0 or π radians.

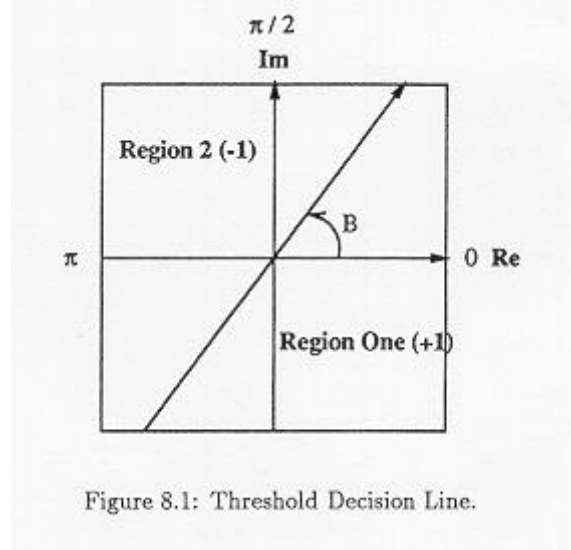


Figure 8.1: Threshold Decision Line.

Figure 8.1 illustrates what is referred to by Downie et al as the 'threshold decision line' [68], defined by angle β , and table 8.1 lists the threshold angle β which is proposed by three different 'camps', those of Horner et al [33], Psaltis et al [69] and Cottrell et al [70].

| Binarisation | β | Phase Angles $\rightarrow 0$ |
|----------------|-------------|--|
| HORNER et al | 0 | $0 \leq \theta \leq \pi$ |
| PSALTIS et al | $[(\pi)/2]$ | $-(\pi)/2 \leq \theta \leq [(\pi)/2]$ |
| COTTRELL et al | $[(\pi)/4]$ | $-(3\pi)/4 \leq \theta \leq [(\pi)/4]$ |

Table 1: Phase binarisation algorithms used

All three algorithms have been well documented and, as shall be described shortly, are used as substages to a new procedure developed in this thesis. A concise review of these algorithms may be found in an article by Dickey, Stalker and Mason [50].

Object Symmetry

As pointed out by Dickey et al [50], the even-odd symmetry of the target object is reflected in the REAL and IMAGINARY parts of the Fourier Transform and thus directly affects the phase. The degree of symmetry of the target object thus has a marked affect on the object's phase spectrum, requiring care in the selection of filter algorithm. This can be seen directly if the Fourier Transform is, in 1-D for simplicity, decomposed into

$$\begin{aligned}
 F_{\text{Re}} &= \int f(x) \cos(vx) dx \\
 F_{\text{Im}} &= - \int f(x) \sin(vx) dx
 \end{aligned} \quad (3)$$

(4)

Thus, for example, an entirely symmetric object (EVEN) has $F_{\text{Im}}=0$. Recall that any REAL 2-D function may be decomposed into both an entirely EVEN and entirely ODD function by the operation

$$\begin{aligned}
f_{\text{EVEN}} &= \frac{1}{2} (f(x)+f(-x)) \\
f_{\text{ODD}} &= \frac{1}{2} (f(x)-f(-x))
\end{aligned} \tag{5}$$

In selecting a threshold angle of $\beta = 0$, the filter of Horner et al is effectively matched to the odd part of the object function. By this, it is meant that a similar target object would produce the exact same binary phase filter if the real parts of both object functions were identical. Psaltis et al, with $\beta = [(\pi)/2]$, choose to match their filter with the even part of the object function. Both these filters then may suffer from false correlations with input objects having similar even and odd parts respectively, as analysed by Barnes et al [71]. The binarisation algorithm of Cottrell et al, with $\beta = [(\pi)/4]$, attempts to combine information from both the EVEN and ODD parts of the object function to decide the final binarised filter phase, and indeed has been shown to reduce false correlations in simulations.

1.2 Optimal Binary Correlation Filters

In contrast to the fixed threshold angle algorithms just described, there exist optimisation techniques which seek to maximise certain characteristic parameters of the correlation (peak height, discrimination, etc.) which operate by varying the angle β . Farn & Goodman [72] have shown that, in 1-D, the optimal correlation for an object which is mostly EVEN corresponds to $\beta \cong [(\pi)/2]$, as might be expected from the discussion immediately above.

Downie et al [68] have performed an optimisation procedure on correlations which use a 2-D binary image of the NASA space shuttle as an input object, a function which in this case was largely EVEN. Experimental results were obtained using 128×128 magneto-optic SLMs as both input and spatial filter. Of interest to this chapter, they found that while in general an off-centre shift in the shuttle (making the object function more ODD) moved the optimally calculated threshold angle away from $[(\pi)/2]$, the change in correlation peak intensity differed only marginally from the $\beta = [(\pi)/2]$ correlation. In fact, the conclusion drawn from there study was that the $\beta = [(\pi)/2]$ threshold angle is 'near optimum for BPOFs for most object functions.' This observation shall be returned to in the next section. However, optimisation procedures are mentioned only for completeness and do not take any further part in the work of this chapter, save for the observation just made.

2 Combined Techniques

2.1 Algorithm Framework

From the initial Fourier Transform data produced by the DFT of a specified target object, one must arrive at a single phase value of either 0 or π radians to assign to each SLM mirror. The spectral phase information from the DFT must somehow be combined so as to form a single phase value which characterises the spectrum over that mirror. This intermediate phase value is called the characteristic phase of the mirror in this project. Following this, a single binary value must be derived from the characteristic phase.

For the moment, let the choices open to us at each stage of the filter calculation be stated without questioning exactly why one might perform some actions.

1. Firstly, we are free to choose whether or not to binarise the initial phases Φ_{ij} of the 9×9 DFT sub-array which describe the spectrum over each mirror.
2. Following this, one must decide upon an appropriate averaging procedure to produce a single phase value, Φ_c , from this data with which to characterise the mirror phase.

3. Finally, one must select an appropriate binarisation algorithm which operates on Φ_c to produce a single mirror phase Φ_m with which to program the SLM.

These three stages form the basis from which all filter calculation performed in this project stems. What effect, one might ask, do the initial and final binarisation stages have on the performance of the correlation filter ? It will be shown that the determination of the characteristic phase allows an answer to this question and further offers the widest choice of filter variability in this investigation.

In the calculation of the characteristic phase, one would like to give more emphasis to those spectral points containing most energy. For instance, if out of two spectral data points on a mirror one contains 10^6 more energy than the other, should one value the phase contributions from each pixel equally ? In computational determination of the characteristic phase, for instance, the FORTRAN function `ATAN2' determines the phase of a complex number irrespective of the magnitude of that number. Therefore if only one `bright' data pixel truly represented the object spectrum over that mirror the phase of this pixel should be given higher priority in determination of the characteristic phase. Thresholding of the initial spectrum to eliminate very low amplitude spatial frequencies could be performed although a mirror dependent threshold algorithm would possibly be required to counter the fact that mirrors in the high spatial frequency region of the spectrum generally receive less energy than those closer to the zero frequency. Thresholding was not used in this project for this reason. To begin with, two rather straightforward methods of determining Φ_c are now described.

2.2 Basic Algorithms

A very straightforward method of forming the characteristic phase of a mirror is the perform an intensity weighted average of Φ_{ij} , followed by binarisation using one of the three algorithms previously described. Care must be taken in this process that the weight assigned to the spatial offset (phase) of a component sinusoid depends only on the intensity (amplitude squared) of that component, and is not influenced by the representation of Φ_{ij} . If a single Fourier component of the object has wavelength λ , so that

$$f(x) = \cos\left(\frac{2\pi}{\lambda}x + \Phi\right) \quad (6)$$

then a phase shift of $\pm[(\pi)/4]$ moves the component spatially to the left or to the right by $[(\lambda)/8]$. The shift to the right ($-[(\pi)/8]$) could equally well be accomplished if the phase were written as $2\pi-[(\pi)/8]$, which would result in an intensity average heavily biased towards initially negative phases. Therefore, in the intensity weighted average of N points,

$$\Phi_c = \frac{\sum_{ij} I_{ij} \Phi_{ij}}{\sum_{ij} I_{ij}} \quad (7)$$

one must ensure that $-\pi < \Phi_{ij} < +\pi$ in order that two offsets of equal magnitude but opposite direction have an equal (but opposite in sign) effect on Φ_c .

Figure 8.2 plots the results of simulations using such a simple phase averaging. Note that the Psaltis final binarisation stage does not appear as filters using this final algorithm were found to be spatially invariant. The ordinate plots percentage peak energy and the abscissa the Gaussian parameter σ (Chapter seven) which best befits description of the data by a 2-D Gaussian function (smaller σ means a sharper peak). The ordinate is

identical with the practical definition of optical efficiency η_p given in chapter seven.

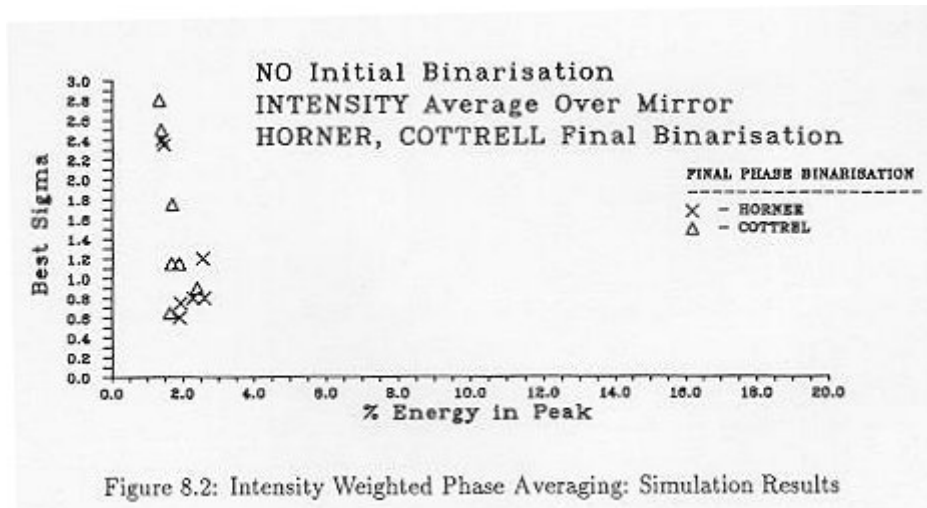


Figure 8.2: Intensity Weighted Phase Averaging: Simulation Results

Figure 8.2: Intensity Weighted Phase Averaging: Simulation Results

It is observed that neither the optical efficiency (percentage energy in peak) nor peak sharpness are particularly inspiring, the reason being the extreme simplicity of the filter algorithm. It will be shown later in this chapter that the phase information of the target objects used is approximated very well by a uniform distribution on the range $-\pi$ to $+\pi$. If, over each mirror, the intensity does not vary rapidly then a large degree of cancellation occurs in equation 8.7 so that the distribution of Φ_c over the 15×15 mirror array is confined to a rather narrow region about $\Phi_c = 0$. Consequently, although the final binarisation algorithm of Horner et al *will* bisect this spread (and Cottrel et al if the distribution is wide enough), the algorithm of Psaltis et al will not. This explains the spatial invariance found in computer simulations of such simple filters using the Psaltis algorithm as a final binarisation stage.

Further, consider the case of a high intensity data point which has a phase of zero. In such a case this point will not contribute anything to the intensity average and thus highlights the limitations of equation 8.7 as a means of determination of characteristic phase. As the characteristic phase was formed by such a simple procedure these results are not of a high standard but are included for comparison with more sophisticated algorithms of this chapter, of which coherent summation is next to be described.

2.3 Coherent Summation

A preferable technique for calculating the characteristic phase is known as 'coherent summation'. In this process, the complex numbers describing the spectrum over any given mirror are, as the name suggests, coherently added together in a process of phasor addition. The phase of the resulting summation, Φ_c , may then be binarised by one of the three algorithms of the preceding subsection. This process has an inbuilt tendency to perform an amplitude weighting of the phase from each data pixel. If one considers the process of diffraction from a single mirror only, the light field at infinity will be approximated by a phasor addition of the complex light field over the mirror, which is where this technique gets its name.

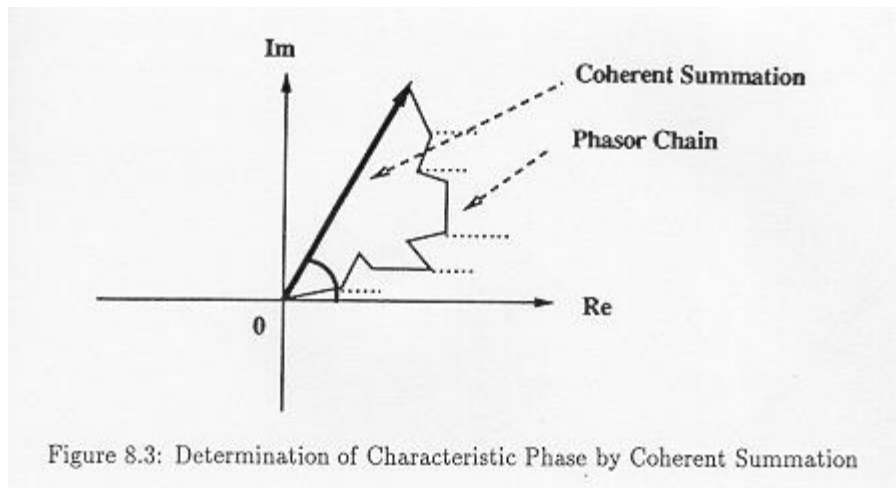


Figure 8.3: Determination of Characteristic Phase by Coherent Summation

This technique enables rapid, straightforward filter calculation and has been used by Flannery et al with the 48×48 magneto-optic SLM. In their calculations a 3×3 sub-array of the DFT was coherently summed and the binarisation algorithm of Horner et al used to obtain the final SLM phases Φ_m . In fitting this process within the framework of general filter calculation, one would say that

1. No initial data binarisation is required.
2. The phase averaging procedure was one of coherent summation.
3. Any final binarisation procedure may be used to obtain Φ_m .

Flannery et al chose to use Horner final binarisation, though it is not stated why preference was given to this over the other two popular algorithms. One can make accurate predictions as to the nature of the filter produced by coherent summation by noting that the phases of each component phasor in the coherent sum are conjugates for conjugate mirrors. Therefore the characteristic phases of conjugate mirrors are necessarily also conjugate. The final binarisation procedure of Horner et al will thus map the phases of a mirror-conjugate pair to opposite poles of zero and π resulting in a filter which is 100% anti-symmetric. By the same reasoning, a final binarisation using the Psaltis algorithm produces a filter of 100% symmetry about the origin. From the threshold line of Cottrell one would expect neither a completely symmetric nor completely anti-symmetric filter. Figure 8.4 illustrates these ideas with the filters produced for the 'C' and 'STAR' objects.

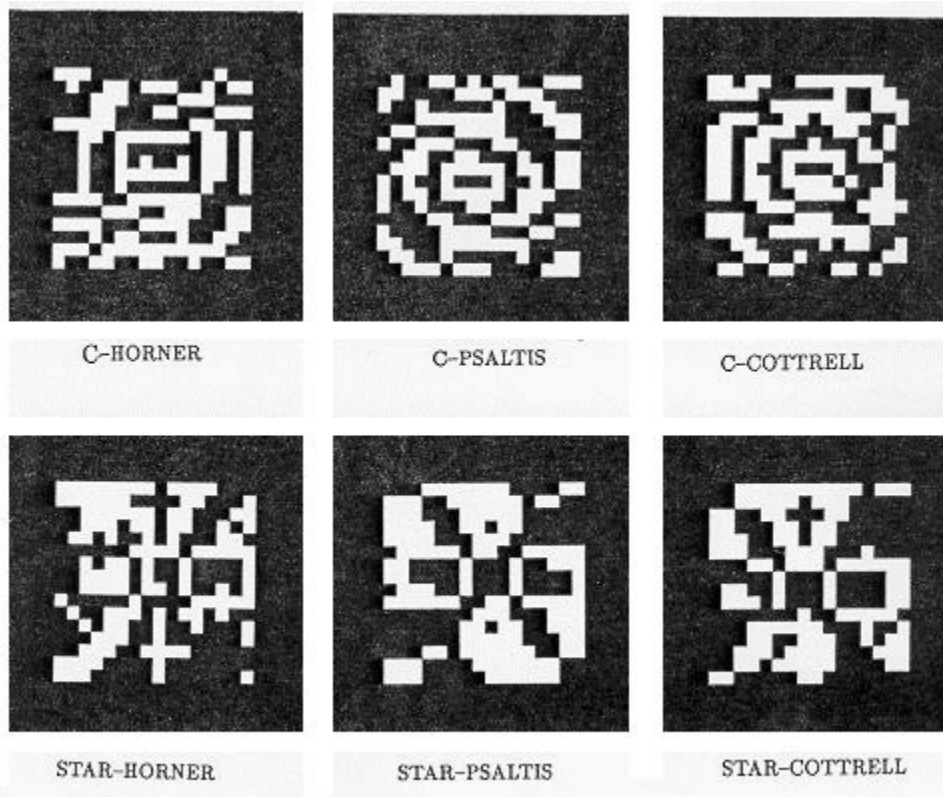


Figure 8.4: Coherent Summation Filters for 'C' and 'STAR'

Figure 8.4: Coherent Summation Filters for 'C' and 'STAR'

Applying a voltage to a mirror, it may be recalled, decreases the optical path length through the liquid crystal as $n_e \rightarrow n_o$ and $n_o > n_e$. Therefore the light from an 'ON' mirror (higher applied voltage) is spatially advanced relative to an 'OFF' mirror. However, when viewed in amplitude modulation mode a mirror with a higher voltage appears *darker* (optical OFF state) and so mirrors shown dark in the above figure have are spatially advanced by $[(\lambda)/2]$ relative to mirrors shown as white.

In the next section, simulation and experimental autocorrelation results obtained from filters produced by two different techniques are compared. The first technique is that of coherent summation just described. The second technique goes under the title of the 'combined' technique, whereby both initial and final data binarisation stages are carried out. Determination of the characteristic phase in the 'combined' technique is by intensity weighted averaging of the (binarised) initial phases. This more general technique is under investigation in this thesis and the results obtained with coherent summation filters are used as a benchmark for comparison. A detailed analysis of 'combined' filters is presented in the final section.

3 Simulation and Experimental Results

Appendix nine provides a brief description of the data capture procedure for the experimental results. Note that great care was taken in the central placement of the objects and in noting the fluctuations of laser intensity. All experimental results of this chapter have been corrected for laser beam fluctuations which in any case amounted to no more than one or two percent of the mean laser output. There are many ways of extracting information from the experimental results as detailed in chapter seven. Figures 8.6 to 8.8 show the experimental auto-correlations obtained using filters produced by coherent summation, as recorded by CCD array camera. Each page shows the result of a single final binarisation algorithm on the coherently summed spectra over each mirror eg. figure 8.6 shows the results of Horner final binarisation and figure 8.7 that of using a Psaltis final binarisation algorithm. The letters beneath each plot denote the target object used in each case.

For comparison, figures 8.9 to 8.11 show the experimental auto-correlations obtained using combined algorithm generated filters. In each case the spectral data over each mirror was initially binarised by either the Horner, Psaltis or Cottrell algorithm, the characteristic phase was then formed by an intensity weighted average of the

binarised phases², and a final mirror phase is chosen by means of the Psaltis algorithm operating on the characteristic phase of each mirror.

A data thresholding operation has been performed to enhance each picture and offset the reduction in contrast which occurs during the hardcopy process. The thresholding operation in question is identical to that used by Hudson et al [73] and is depicted in figure 8.5.

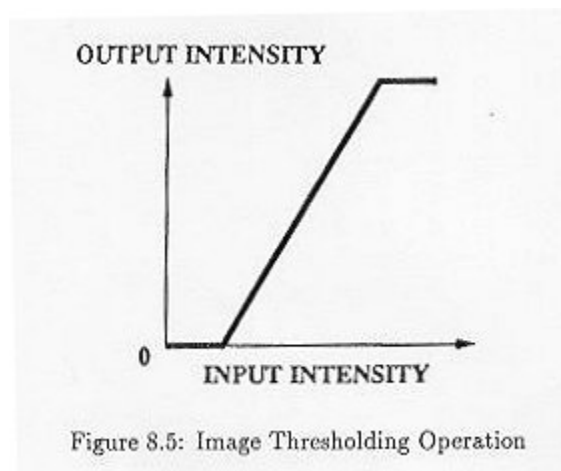


Figure 8.5: Image Thresholding Operation

Such operations have also been performed by Flannery et al [44] by optimisation of their video display controls where it is realised that basic post-processing of this kind will usually be required in experimental correlator systems. Appendix nine provides a comparison of the hardcopies obtained both with and without the thresholding operation.

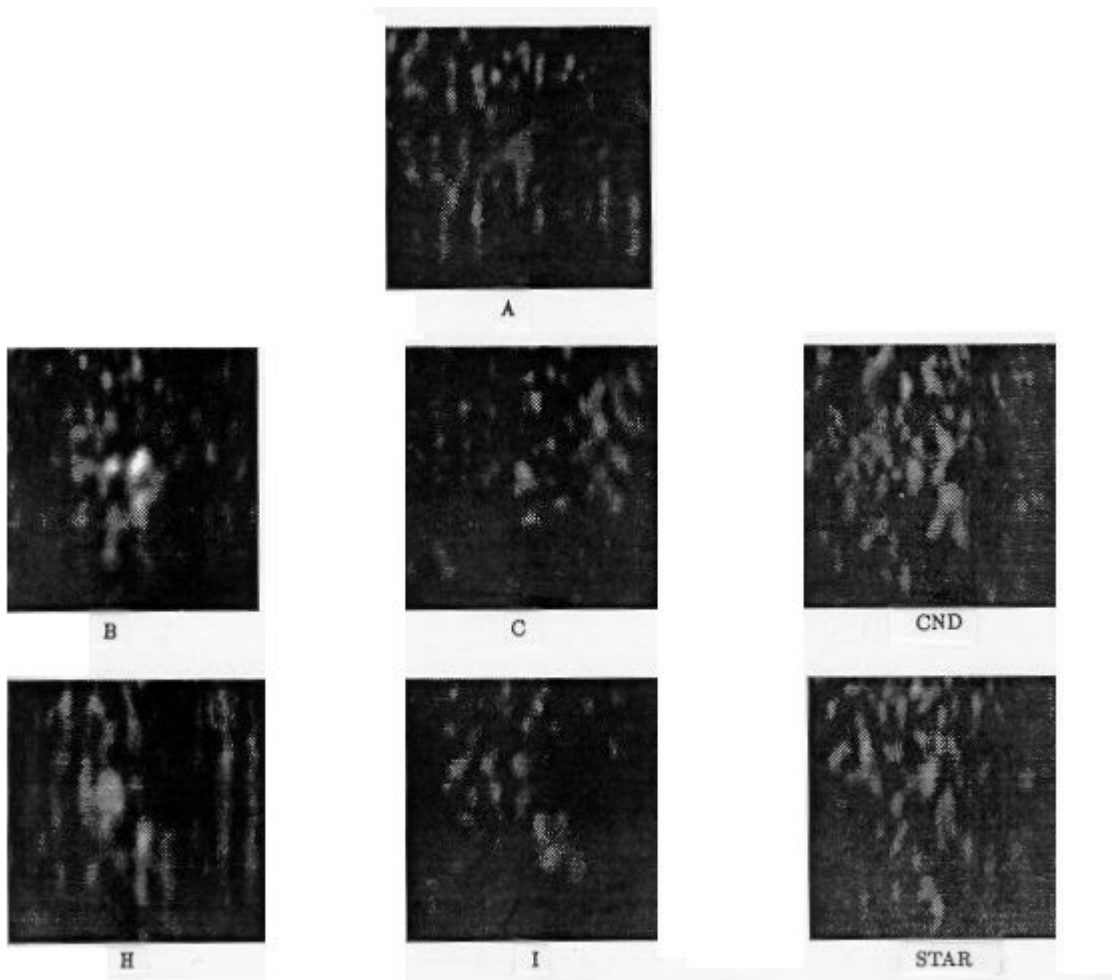


Figure 8.6: Coherent Summation: Horner Final Binarisation

Figure 8.6: Coherent Summation: Horner Final Binarisation

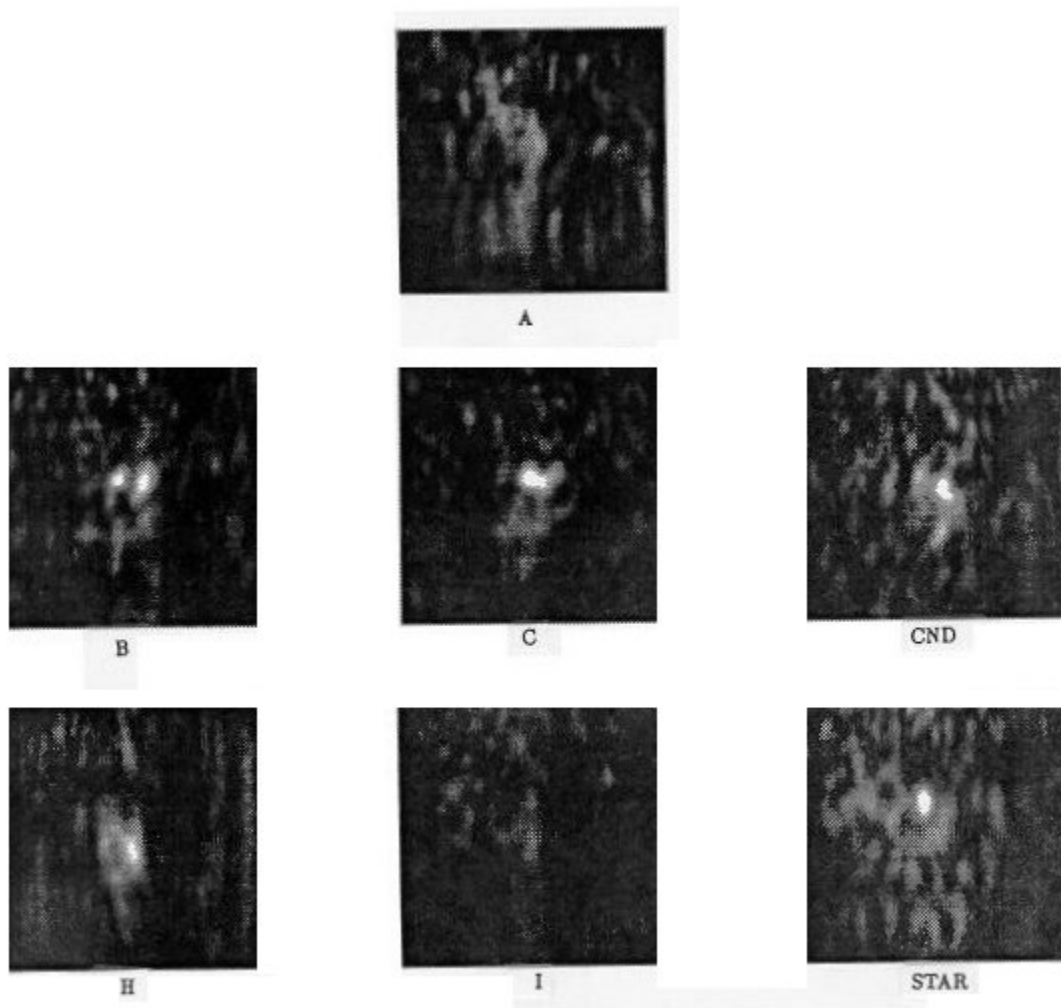


Figure 8.7: Coherent Summation: Psaltis Final Binarisation

Figure 8.7: Coherent Summation: Psaltis Final Binarisation

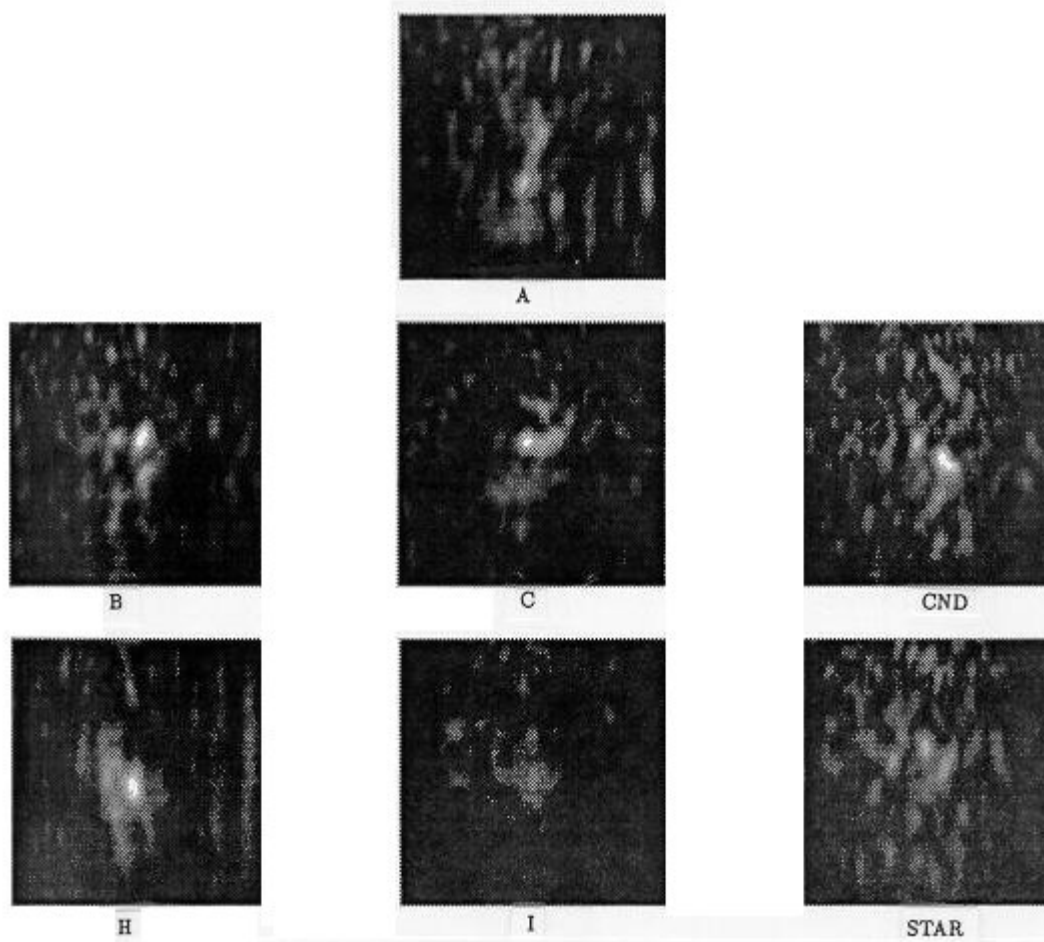


Figure 8.8: Coherent Summation: Cottrel Final Binarisation

Figure 8.8: Coherent Summation: Cottrel Final Binarisation

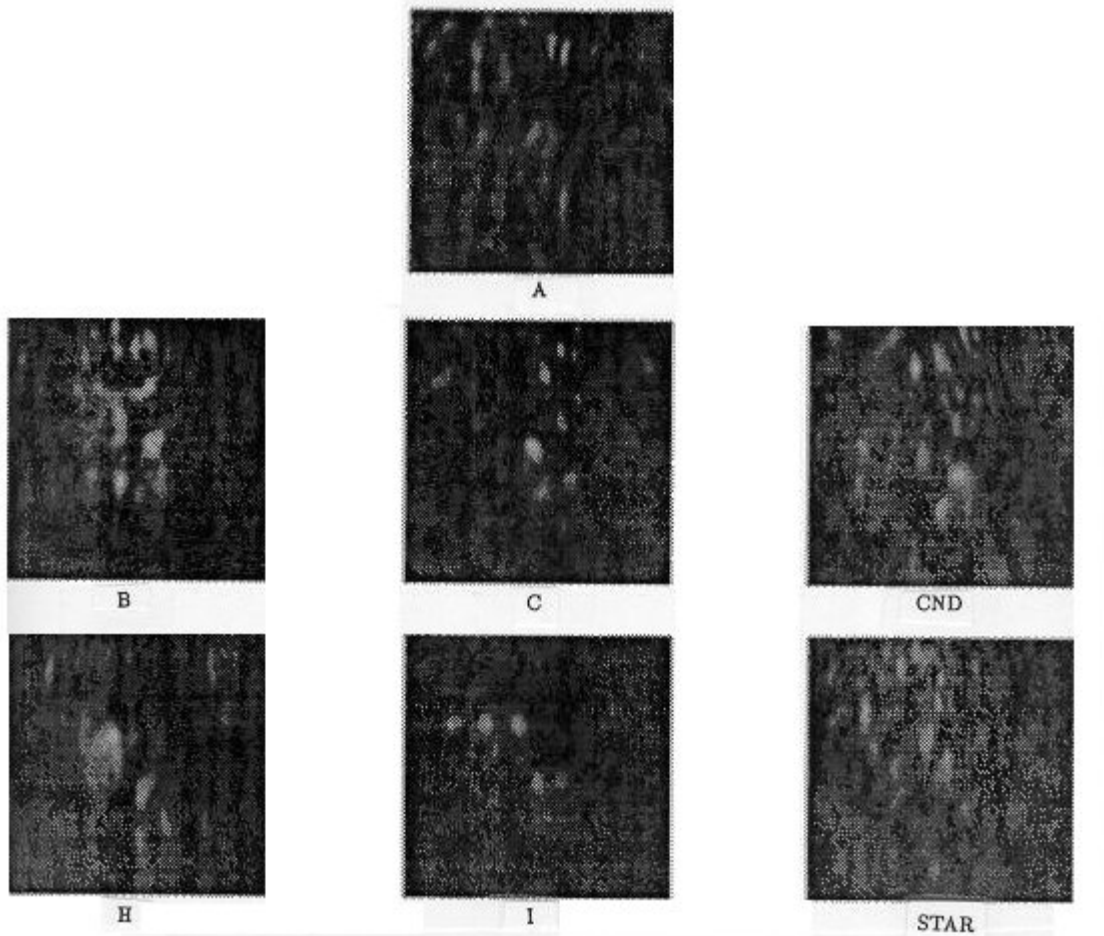


Figure 8.9: Combined Algorithms: Horner Initial Binarisation, Intensity weighted Average Φ_c , Psaltis Final Binarisation

Figure 8.9: Combined Algorithms: Horner Initial Binarisation, Intensity weighted Average Φ_c , Psaltis Final Binarisation



Figure 8.10: Combined Algorithms: Psaltis Initial Binarisation, Intensity weighted Average Φ_c , Psaltis Final Binarisation

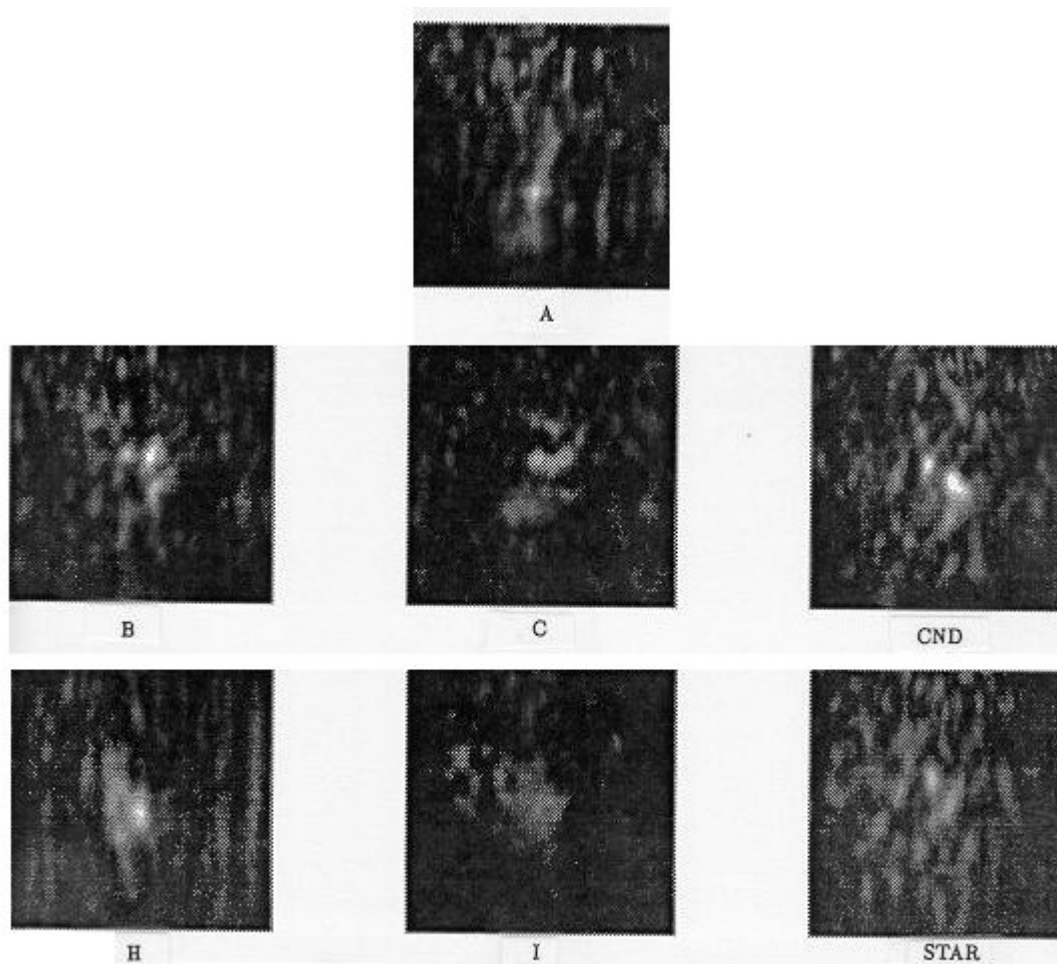


Figure 8.11: Combined Algorithms: Cottrell Initial Binarisation, Intensity weighted Average Φ_c , Psaltis Final Binarisation

Figure 8.11: Combined Algorithms: Cottrell Initial Binarisation, Intensity weighted Average Φ_c , Psaltis Final Binarisation

Observations

1. Firstly, something very much like an auto-correlation peak is found close to the centre of each image for many of the filters. Certainly no image resembles that of the corresponding target object which would result from a constant phase assigned to each mirror of the SLM. In many cases the image does not contain a single peak and certainly suffers from a considerable amount of noise even after thresholding.
2. Of those filters produced via coherent summation, Psaltis final stage binarisation produces considerably brighter, more distinct correlation peaks. Recall the conclusions of Downie et al [68] which also found the Psaltis final binarisation algorithm to be the most effective.
3. Filters produced with the combined technique, encompassing intensity weighted determination of the characteristic phase, may be characterised by noting that the auto-correlation is worst for Horner initial binarisation, very good on the whole for Psaltis initial binarisation, and not quite as good for Cottrell initial binarisation. Estimation of quality is based on visual inspection of peak intensity, number of sub-peaks and the distribution of energy between all peak-like features in each image.
4. It is observed that of the two filter computation processes used, equivalent filters³ produced broadly similar results. During the course of the experiment the filters were cycled through the SLM in turn for each object so that slight object misplacement effects were identical for each. The change in autocorrelation observed on the video monitor in switching between a combined filter and the equivalent coherent summation filter was extremely slight, although a definite change was registered.

- For both combined and coherent summation filters, the results for the 'I' target object are very poor. Speculation as to the cause of this will be returned to shortly upon a quantitative analysis of these results and comparison with simulation. Note, however, that the experiment was carried out on a number of different objects to reduce the danger of carrying all one's eggs in the same basket. For example, it may be that the high symmetry of the object reduces the algorithm efficiency as inspection of the 'H' auto-correlations might also suggest. An analysis based on the results from two such objects would not yield results of general validity.

Figure 8.12 plots the experimental correlation peaks arising from Horner, Psaltis and Cottrell initial binarisation, intensity weighted Φ_c and Psaltis final binarisation for the 'C' target object. This object was chosen as it is neither the best nor the worst result and shows the clear central peak obtained from the algorithm expected to perform best, that of Psaltis initial binarisation, where no energy would lie were the image merely an inverted letter 'C'.

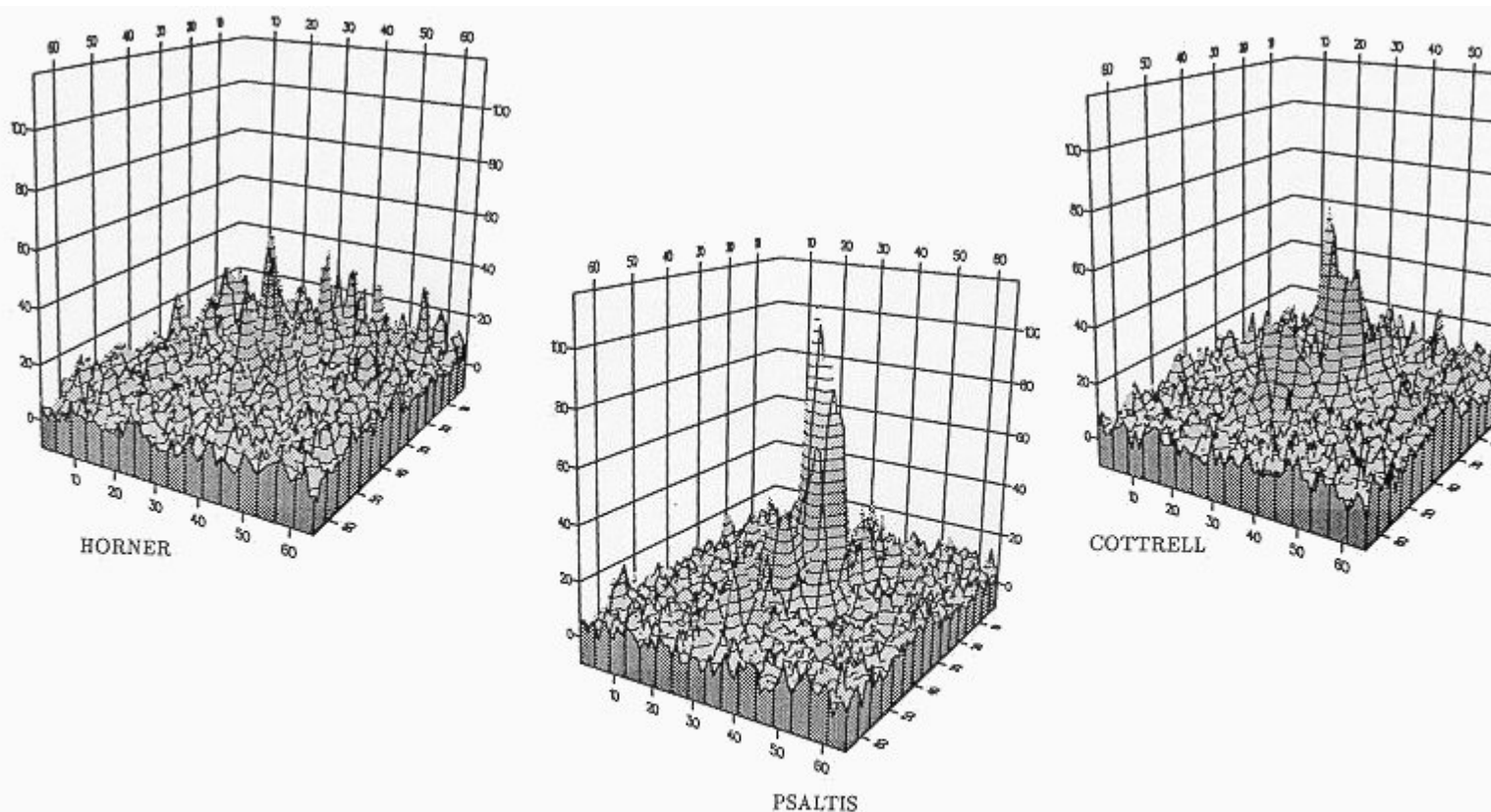


Figure 8.12: 3-D Contour Graphs of Auto-correlations using the 'C' Target.
(Combined Algorithm Filter Results.)

Figure 8.12: 3-D Contour Graphs of Auto-correlations using the 'C' Target. (Combined Algorithm Filter Results.)

3.1 Quantitative Analysis

After initial data capture by CCD and PC based framegrabber the data was transferred to a DEC microvax computer for analysis. A comprehensive FORTRAN data examination program used the voltage information from a photodiode in the object plane (illuminated alongside the object) to correct the data for laser beam fluctuations, as detailed in appendix nine. A search was then instigated to locate the position of the maximum pixel value. Assuming this to be an auto-correlation peak, the best fitting Gaussian curve is fitted to the data and the percentage peak-to-total energy of the data is also computed. Figures 8.6 to 8.11 show that this assumption is not valid for filters using the Horner binarisation algorithm, whether the filter be coherent summation based or combined algorithm based. Therefore, the scatter plots of peak sharpness σ to percentage peak energy *must* be viewed in relation to these visual correlation plots.

Figure 8.13 shows scatter graphs of percentage peak energy to peak sharpness for every filter used in this project. Both simulation results and experimental results are displayed for convenient cross-comparison. The array camera field of view is equivalent to $\cong 1.7\text{mm}$ on a side so that the CCD array just picks out one replication⁴ of the correlation peak in the image plane (Recall the target objects are $\cong 1.9\text{mm}$ on a side). Note that the areas used to collect the energy are therefore slightly different between simulation and experiment, but that this should cause no difficulty if it is remembered only to compare correlation peak characterisation parameters arising from different filters within the simulation results or the experimental results obtained, but not between the two.

Appendix nine provides an example of the fitted Gaussian over an auto-correlation peak so that the reader may judge the validity of σ as a peak characterisation parameter.

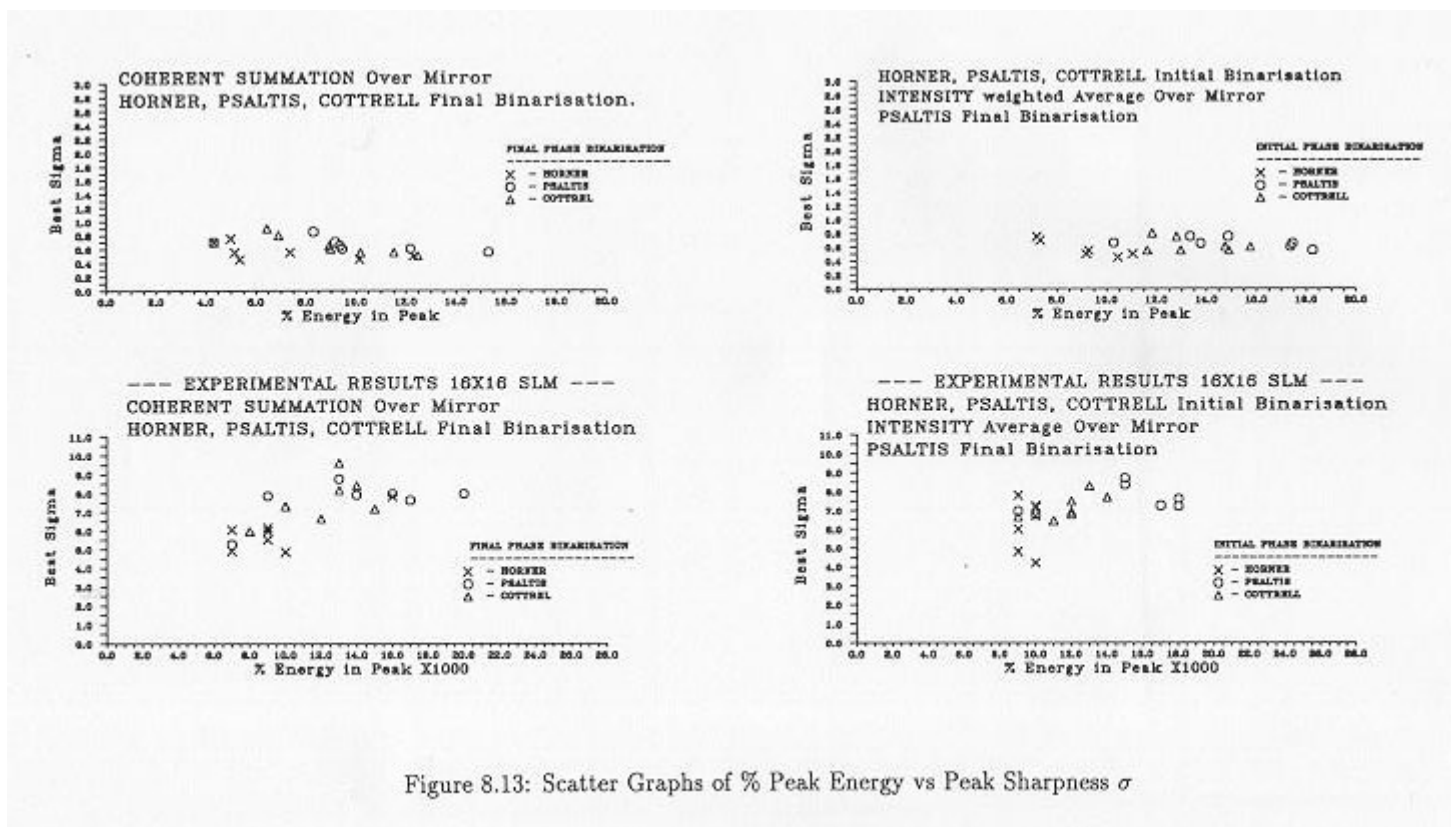


Figure 8.13: Scatter Graphs of % Peak Energy vs Peak Sharpness σ

Figure 8.13: Scatter Graphs of % Peak Energy vs Peak Sharpness σ

Scatter Graph Observations

Coherent Summation

1. In both simulation and experiment similar trends are found. Horner final binarisation generally has the lowest peak energy but tends also to be the sharpest. From the CCD hardcopy figures however it is clear that filters with Horner final binarisation produce no clear correlation peak⁵ and such data should be excluded from comparison with the other final binarisation algorithms.
2. Although considerable overlap exists, it is found that Cottrell final binarisation produces a marginally less bright peak than Psaltis final binarisation for both simulation and experimental results.

Combined Technique

1. The general observations made for coherent summation also apply for these results. However, the distinction between results from filters using different initial data binarisation is greater than for coherent summation.
2. It is evident from the graphs that Psaltis initial binarisation produces, on the whole, a brighter peak of

approximately equal sharpness to Cottrell initial binarisation.

A final analysis of the data is effected by performing a one-to-one comparison of the percentage peak energy between simulation and experiment, for each object, as shown in figure 8.14.

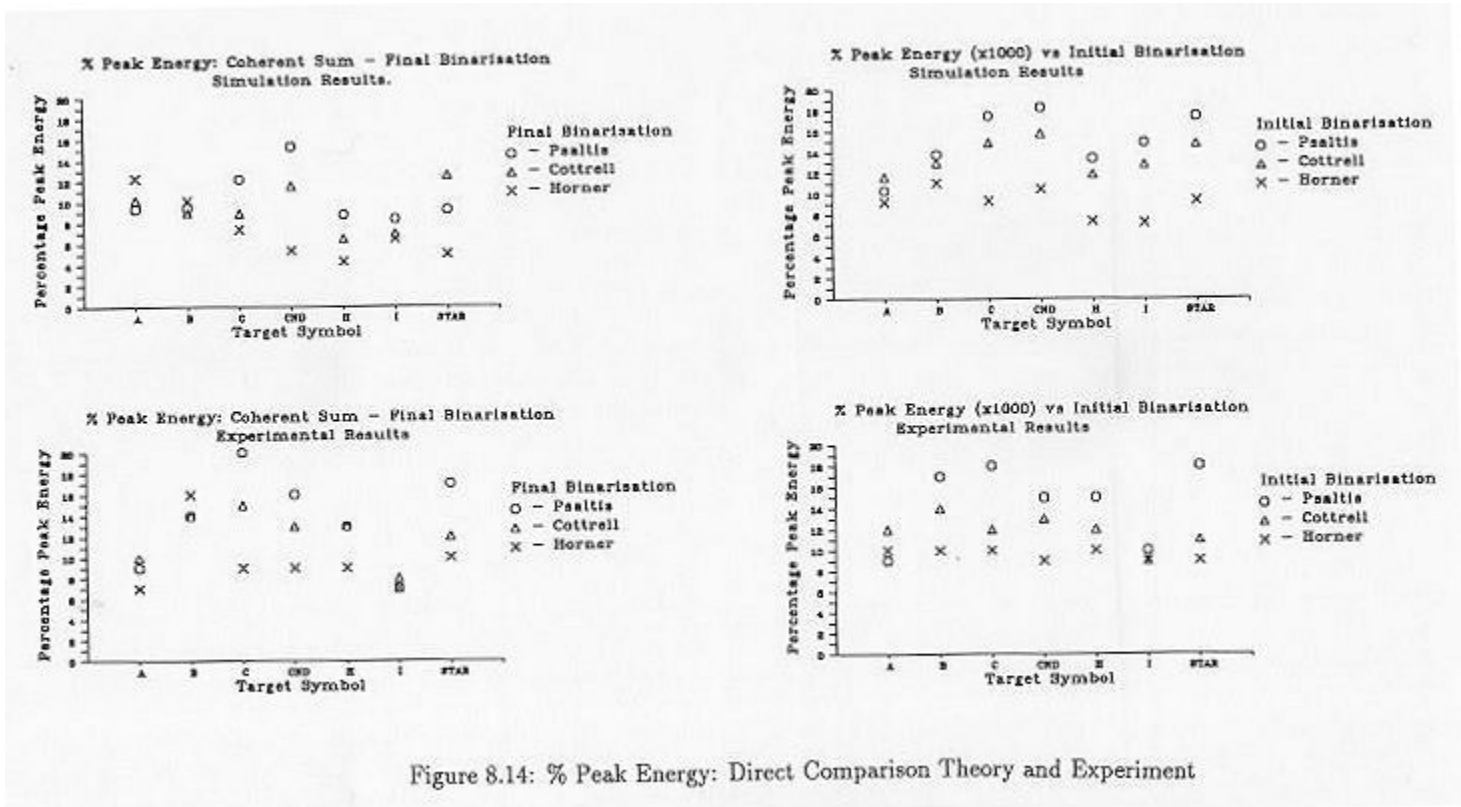


Figure 8.14: % Peak Energy: Direct Comparison Theory and Experiment

Figure 8.14: % Peak Energy: Direct Comparison Theory and Experiment

This method of data analysis is more direct than the scatter graph approach and, if the Horner data is not compared with the other binarisation algorithms, shows solid agreement for the combined technique between simulation and experiment. In all cases the Psaltis initial binarisation resulted in an equal or, more usually, brighter correlation peak than that of Cottrell initial binarisation. If one does choose to look at the results of Horner initial binarisation one can only say that both simulation and experiment agree the correlation resulting is extremely poor. Note again that this is not a reflection of the actual Horner algorithm merit, but arises from the nature of the combined process as previously detailed.

For coherent summation, in simulations the percentage peak energy for the object 'I' is low, but comparable with the lowest Psaltis and Cottrell percentage peak energies of other target objects. The significantly lower peak energy of the 'I' experimental results relative to the other target objects might suggest the actual fabricated object was somehow imperfect rather than an algorithmic weakness. For the intensity weighted Φ_c algorithm, simulations find the percentage peak energy lies approximately midway between the highest and lowest of all simulations (again discounting Horner initial binarisation) which again suggests the fabricated test object suffered some imperfection during manufacture due to the large experimental discrepancy relative to the other targets.

The results of coherent summation are again in strong agreement between simulation and experiment. In only one case, that of the 'STAR' object, does the simulation actually predict that Cottrell final binarisation produces a brighter peak than that of Psaltis. Experimentally the Psaltis final binarisation is a clear winner for this object however. If one accepts the possibility that slight object scaling errors during manufacture, together with different random phase noise for each target object manufactured, may cause object dependent differences between simulation and experiment then this result should not cause too much concern. On the contrary, it is the degree to which simulation and experiment are in agreement which is the most significant result.

3.2 Discrimination Ability

Figure 8.15 displays the first correlation experiment results ever performed with the 16×16 SLM in FIB mode by Ranshaw. Ranshaw's experiment used a square target object, the phase of the Fourier Transform being already binary and avoiding the need for extensive binarisation algorithm research.

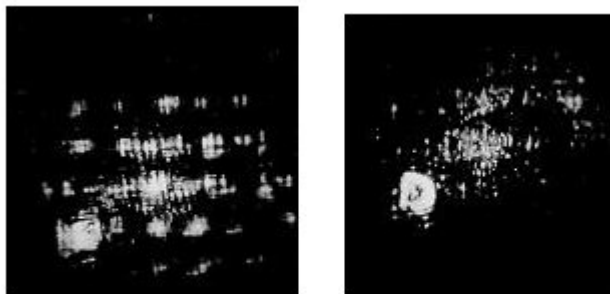


Figure 8.15: Auto and Cross-correlation Results of Ranshaw

Figure 8.15: Auto and Cross-correlation Results of Ranshaw

On the left of figure 8.15 is the autocorrelation of the square target object and on the right the cross-correlation with a letter `D'. The cross-correlation shows significant reduction in the replication intensities, even though they may only loosely be described as `peaks' in the auto-correlation. The front face reflection is clearly visible in both photographs. It was these photographs which prompted the Spatial Light Modulator research part of this project, and they are included to illustrate the potential improvement in this field by intensive algorithm research and improved device fabrication techniques.

A limited experimental investigation into the discrimination ability of the algorithms used on the 16×16 SLM was conducted. The best filter for the letter `A' (Psaltis initial and final binarisation and intensity weighted determination of the characteristic phase) was selected whilst the target object used was varied. Figure 8.16 depicts the intensity distributions in the image plane for the `B', `C' and `CND' target objects with image plane thresholding.

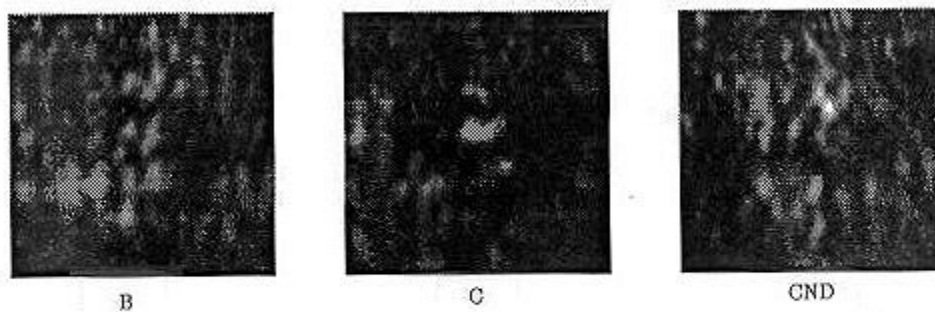


Figure 8.16: Discrimination for `B', `C' and `CND' Target Objects. Combined algorithm filter for the letter `A'.

Figure 8.16: Discrimination for `B', `C' and `CND' Target Objects. Combined algorithm filter for the letter `A'.

These results were typical of those generally obtained for which simulations show contain a percentage peak energy of at most 3%. Notice, however, that the arms of the `CND' symbol result in a strong cross-correlation with the letter `A' in figure 8.16.. Study into filter discrimination is in itself a substantial task and was not pursued further in this project. The experimental results do, however, show that the filter algorithms chosen for use with the 16×16 SLM are both capable of generating both good object recognition characteristics and discrimination ability given the limited space-bandwidth product of the device.

4 Analysis of Combined Technique

4.1 Initial Phase Binarisation

Initial binarisation of Φ_{ij} naturally has a strong influence on the characteristic phase produced from such data. In this subsection it will be ascertained that the characteristic phase resulting from an intensity weighted average of the binarised initial data Φ_{ij} does, in fact, strongly represent the results of the initial binarisation operation. Filter performance, it shall be shown, may in part be speculated upon by consideration of the symmetry of the filter about the origin.

It must be stressed that the analysis performed in this section relates only to binarisation algorithms which use 0 and π radians as the poles of the algorithm. The analysis presented is invalid should one choose poles such as $-(\pi/2)$ and $+(\pi/2)$ and therefore cannot be generalised to the case of general pole values. However, for the specific poles chosen (which are as valid as any) the analysis provides a detailed explanation of the filter characteristics and provides an explanation as to the differing performance of filters produced using the combined technique.

Over an arbitrary SLM mirror, let the subset of initial phase information set to 0 be denoted as set 'A', and those pixels set to π radians be denoted as set 'B'. The characteristic phase is most readily formed by an intensity weighted average of the binarised initial

$$\Phi_c = \frac{\sum_B I_{ij} \pi}{\sum_{A+B} I_{ij}} \quad (8)$$

where I_{ij} denotes the intensity of one pixel within the 9×9 DFT sub-array over the mirror in question. In order to proceed one must make certain approximations about the light distribution over the mirror, the first of which concerns the intensity. It is proposed that the intensity be replaced by an average value over that mirror so that $I_{ij} \rightarrow [\bar{I}]$. This approximation is most easily validated in cases where the scale of Fourier Transform is such that the frequency range covered by any mirror is relatively small, so that the intensity variations over a mirror will also, hopefully, be small. If n_A and n_B denote the number of points in sets A and B respectively the characteristic phase reduces to

$$\Phi_c \cong \frac{n_B}{n_A + n_B} \pi \quad (9)$$

Therefore, if initial data binarisation is used followed by an intensity weighted average of the (binarised) phases, one obtains a characteristic phase which is linearly proportional to the percentage of initial data set to π . Whatever the criteria used by the initial binarisation algorithm to set phase to π , it might be argued that the characteristic phase should reflect the results of this algorithm and, with the procedure outlined here, just such a characteristic phase occurs. Note that the approximation of a slowly varying intensity over the mirror is a sufficient though not a necessary condition for replacing I_{ij} with a mean value. If, for instance, the intensity changes rapidly over the mirror so that

$$I_{ij} = \bar{I} + \delta I_{ij} \quad (10)$$

then, if δI_{ij} is a function with a mean value close to zero, equation 8.9 remains unchanged. Sight must not be lost on the fact that the approximations made here are but guides through the filter calculation process.

Distribution of Φ_{ij}

The second approximation of this analysis relates to determination of n_A and n_B of equation 8.9, which in turn will determine the plausibility of the explanation of the combined technique. What would happen if $n_B=0$, for instance? From chapter five it will be recalled that the importance of the phase information of a spectrum far outweighs the amplitude information and it is also known that the average amplitude spectrum of an input scene to an optical system is accurately described by a Gaussian function. If the amplitude spectra of, say, 100 typical input scenes were replaced with a common suitable Gaussian function the phase information present in the frequency plane would be enough to allow a recognizable image of each object in the image plane.

This observation relies on the fact that the uniqueness of each object is related to the uniqueness of its associated phase spectrum, which may sound like stating the obvious. However, given that the phase spectra is unique to each object, it is a logical conclusion that if one were to pick the phase of an arbitrary spatial frequency of an arbitrary object it could lie anywhere on the range $-\pi$ to $+\pi$ i.e it is a random variable with a uniform probability distribution⁶.

If this is true, then any threshold angle β chosen for an initial data binarisation should set approximately half of the phases to 0 and half to π . Table 8.2 lists the percentage of Φ_{ij} set to π radians for the SLM as a whole, for just two of the seven target objects used.

| Object | Initial Binarisation | % $\rightarrow \pi$ |
|--------|----------------------|---------------------|
| A | Horner et al | 49.80% |
| | Psaltis et al | 49.86% |
| | Cottrell et al | 49.82% |
| C | Horner et al | 49.80% |
| | Psaltis et al | 49.79% |
| | Cottrell et al | 49.76% |

Table 2: Percentage of Φ_{ij} set to π for 'A' and 'C' Target Objects

In fact, every target object showed identical results to those of this table. Percentages are always on the lower side of 50% due to a programming decision which maps all phases which actually lie on the threshold line to a phase of zero. Based on the results such as those of table 8.2, the assumption of a rather uniform distribution of Φ_{ij} would seem valid for the target objects used in this project and valid in general for almost every (non-symmetric) target object likely to be used in a realistic correlator. The conclusion is therefore that n_B is most unlikely to be zero for all practical target objects.

In relation to the problem at hand, both sets A and B contain approximately half of the total number of data pixels over any one mirror which leads to the result that

$$\Phi_c \cong \frac{\pi}{2} \quad (11)$$

Therefore, for the seven target objects used in this project, one might expect the characteristic phases of each mirror of the SLM to be closely distributed about the value $[(\pi)/2]$.

Effects of the Characteristic Phase

Recall the three threshold angles β introduced so far. If the characteristic phases of the SLM mirrors are closely distributed about $[(\pi)/2]$ then only the threshold line of Psaltis et al will divide this distribution, as figure 8.17 depicts.

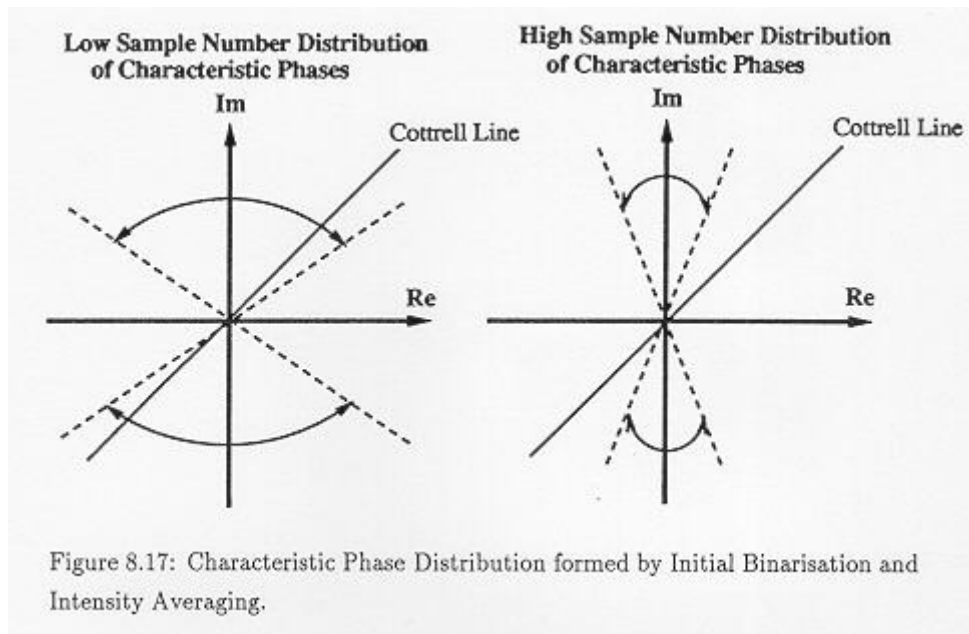


Figure 8.17: Characteristic Phase Distribution formed by Initial Binarisation and Intensity Averaging.

The threshold lines of Horner et al and Cottrell et al have all characteristic phases lying in just one of their two distinguishable regions and thus would produce filters where Φ_m does not vary from mirror to mirror, as has been verified to occur in simulations carried out for this project. To recap on the filter formation process then,

1. On any mirror the 9×9 DFT sub-array is phase binarised by any of the three algorithms used in this chapter.
2. An intensity weighted average of the binarised phases leads to a characteristic phase Φ_c which is a fraction of π .
3. The characteristic phase approaches π in proportion to the initial fraction of data which was binarised to π . Using the assumption of an initially almost uniform distribution of Φ_{ij} on the range $-\pi, +\pi$ one must conclude that Φ_c is clustered around the value $[(\pi)/2]$.
4. Upon final binarisation of Φ_c only the algorithm of Psaltis et al can produce a filter with mirror phases Φ_m which are not all identical due to the tight clustering described above. If Φ_c is such that it is approximately evenly distributed about $[(\pi)/2]$ then $\cong 50\%$ of the final filter has mirror phases Φ_m set to 0 and $\cong 50\%$ to π .

Table 8.3 shows the extent to which this explanation is plausible by listing the percentages of mirrors which have a final phase Φ_m set to π .

| Initial Binarisation | A | B | C | CND | H | I | STAR |
|----------------------|------|------|------|------|------|------|------|
| Horner et al | 58.7 | 48.4 | 48.8 | 47.3 | 48.0 | 49.2 | 47.3 |
| Psaltis et al | 49.2 | 44.4 | 54.3 | 45.7 | 43.4 | 41.4 | 51.6 |
| Cottrell et al | 48.8 | 50.0 | 49.6 | 49.6 | 48.6 | 43.8 | 49.2 |

Table 3: Percentage of Mirrors set to π vs Initial Binarisation (Intensity Weighted Average then Psaltis Final Binarisation).

So far, no criterion has been established to predict how well each filter will perform as a binary phase-only filter for optical correlation work. It is the analysis of filter symmetry which provides clues as to filter performance, as shall now be shown.

4.2 Filter Symmetry

Consider a single mirror M of the SLM which is represented by a 9×9 sub-array of DFT points, each with intensity I_{ij} and phase Φ_{ij} . The symmetry of the filter as a whole may be calculated by considering also the conjugate mirror to M which is M^* . By definition of the Fourier Transform, a point on M with intensity I_{ij} and phase Φ_{ij} has a conjugate point on M^* with equal amplitude but conjugate phase $-\Phi_{ij}$. Figure 8.18 depicts on an Argand diagram the phase of four data points on both M and M^* , where it is noted that phase conjugation is equivalent to reflection about the REAL axis.

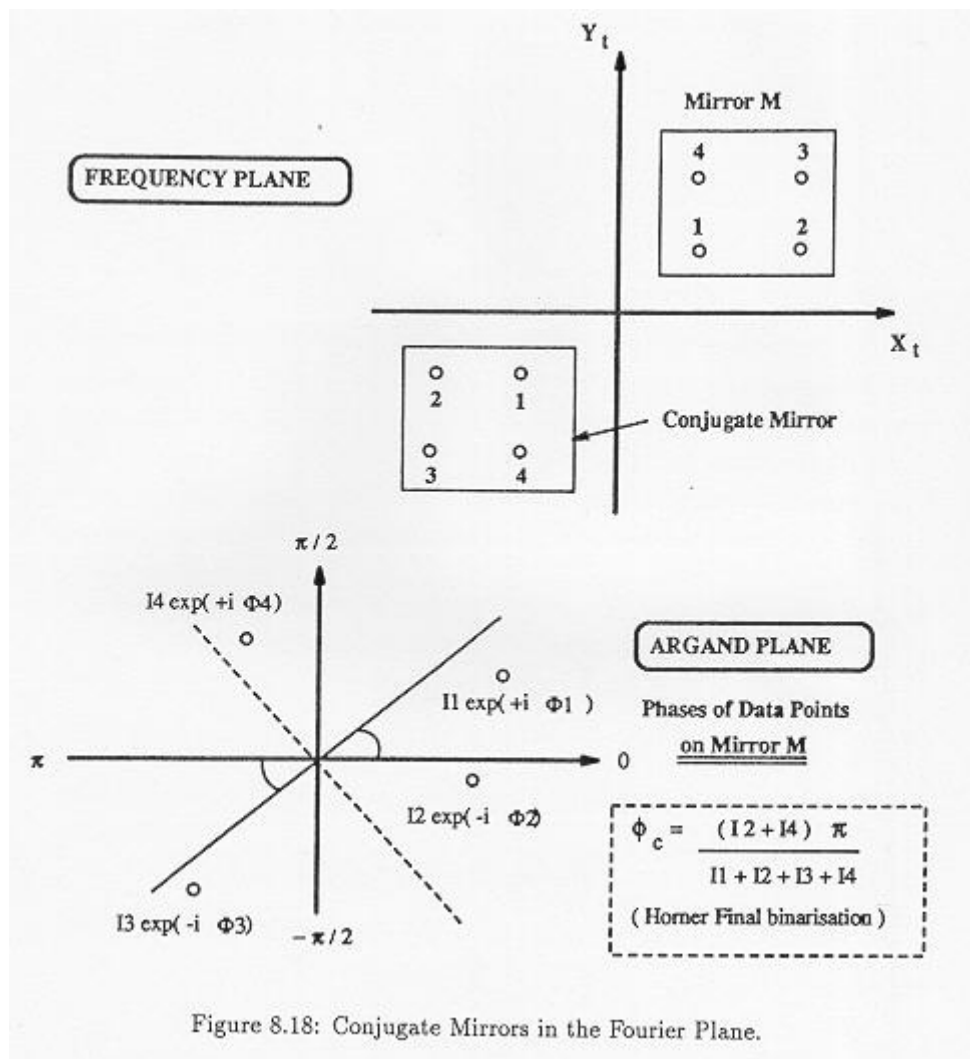


Figure 8.18: Conjugate Mirrors in the Fourier Plane.

Recall that set B denotes those points which are mapped to a phase of π (and is used in determining Φ_c), and set A those points mapped to a phase of 0. Table 8.4 defines these sets for the three binarisation algorithms of this chapter for both M and M^* , taking the phases shown in the figure for example.

| Binarisation Algorithm | Mirror M | | Mirror M^* | |
|------------------------|----------|-------|--------------|-------|
| | Set A | Set B | Set A | Set B |
| Horner et al | 1,4 | 2,3 | 2,3 | 1,4 |
| Psaltis et al | 1,2 | 3,4 | 1,2 | 3,4 |
| Cottrell et al | 1,2,3 | 4 | 1,2,4 | 3 |

Table 4: Mapping Sets for the Binarisation Algorithms of this Chapter.

Horner Initial Binarisation

Consider the phase mapping of the Horner algorithm on the data points of both mirrors. From table 8.4 it is apparent that set B for mirror M is identical to set A for mirror M* and vice versa. As only the information from set B takes part in the formation of the characteristic phase for each mirror it is further apparent that in its calculation $\Phi_c(M^*)$ uses a mutually exclusive data set than does $\Phi_c(M)$. Thus, from equation 8.9, the characteristic phase of one mirror has absolutely no relation at all with the characteristic phase of the conjugate mirror, and one might expect a corresponding filter performance of dubious quality to result.

It is not immediately apparent that the fact that mutually exclusive data sets are used for conjugate mirrors results in a filter which is completely anti-symmetric. For mirror M, the characteristic phase is found from

$$\Phi_c(M) = \frac{\sum_B I_{ij} \pi}{\sum_{A+B} I_{ij}} \quad (12)$$

and, if A and B again refer to the sets of mirror M, the characteristic phase of mirror M* is

$$\Phi_c(M^*) = \frac{\sum_A I_{ij} \pi}{\sum_{A+B} I_{ij}} \quad (13)$$

However, one may write

$$\sum_A I_{ij} = \sum_{A+B} I_{ij} - \sum_B I_{ij} \quad (14)$$

so that

$$\Phi_c(M^*) = \pi - \Phi_c(M) \quad (15)$$

From earlier work it is known that $\Phi_c(M)$ is closely distributed about $[(\pi)/2]$ so that if one writes

$$\Phi_c(M) = \frac{\pi}{2} \pm \delta \quad (16)$$

then

$$\Phi_c(M^*) = \frac{\pi}{2} - \pm \delta \quad (17)$$

Therefore, the characteristic phases of conjugate mirrors lie on opposite sides of the imaginary axis and will be binarised to different poles by the Psaltis final binarisation algorithm. An entirely anti-symmetric filter must then

result no matter what target object is used.

Psaltis Initial Binarisation

Now consider the effects of using the initial binarisation of Psaltis et al where the threshold line coincides with the imaginary axis of figure 8.18. Set B now comprises all points to the left of the imaginary axis and as conjugation is effected by reflection in the REAL axis, set B is identical for both M and M^* . Therefore as the characteristic phases for a mirror and its conjugate are identical, the final binarisation algorithm must give an identical output phase for both mirrors and the filter will be 100% symmetrical about the origin. Only half of the information contained in each mirror (those points with phases to the left of the Imaginary axis in the Argand plane) is used to form the characteristic phase but this information is the same for conjugate mirrors.

Cottrell Initial Binarisation

Assuming a uniform distribution of phases Φ_{ij} , the threshold line of Cottrell et al results in set B of mirror M^* using 50% of the information used to compute the characteristic phase of mirror M, and 50% of previously unused data. Figure 8.19 aids this discussion. Initial binarisation using the algorithm of Cottrell et al followed by an intensity weighted average of the binarised phases is a procedure which therefore lies midway between the previous two initial binarisation algorithms in as much as analysis of the characteristic phase is concerned.

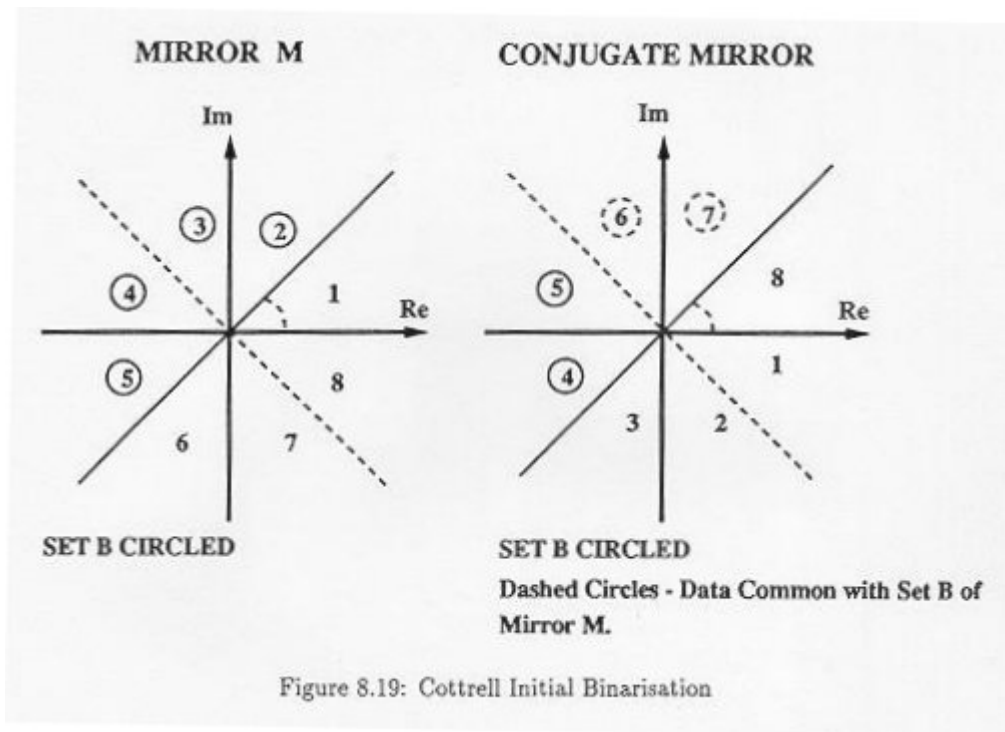


Figure 8.19: Cottrell Initial Binarisation

twice per cycle of the lens cut-off frequency. As such, one might expect the filter to be neither completely symmetric nor completely anti-symmetric after the final Psaltis binarisation algorithm is applied to the characteristic phases. Further, if the filter resulting from Horner initial binarisation is suspected to give poor results, and that arising from Psaltis initial binarisation rather better results, one might expect the filter in question to lie in between these two extremes in terms of correlation quality.

It should be noted that expectations expounded here of filter performance are based solely on the dependence of Φ_c on the choice of data sets used in its calculation. However, the approximations and reasoning used so far have led to an in depth analysis of filter symmetry expected to occur from the filter creation process framework at the beginning of this section. Figure 8.20 shows several filters calculated using this combined algorithm technique, these being typical of the results obtained for all test objects used. For the 'star' target object the filter pattern is also shown as it appears on the 16x16 SLM, in amplitude mode. Remember that the top row and left column are

not required for symmetric placing of the SLM in the frequency plane, and should be excluded from visual estimations of symmetry. The same mirror phase calculation is performed for these mirrors (from a reduced data set) nonetheless. Note the similarity between these filters and those as calculated by coherent summation.

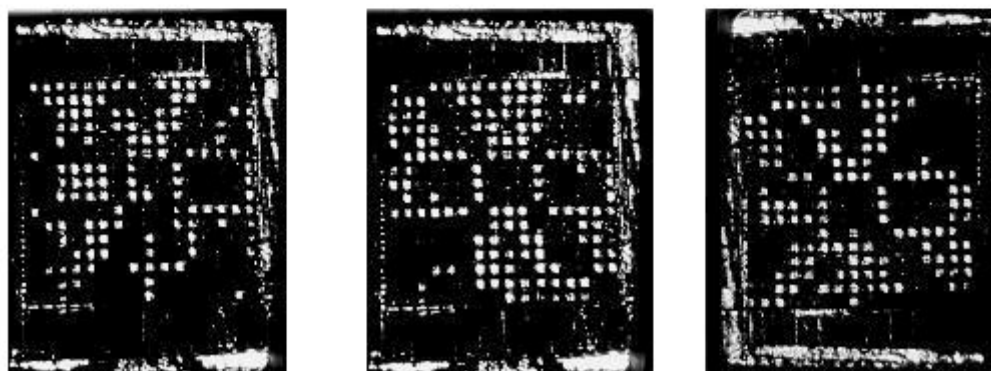
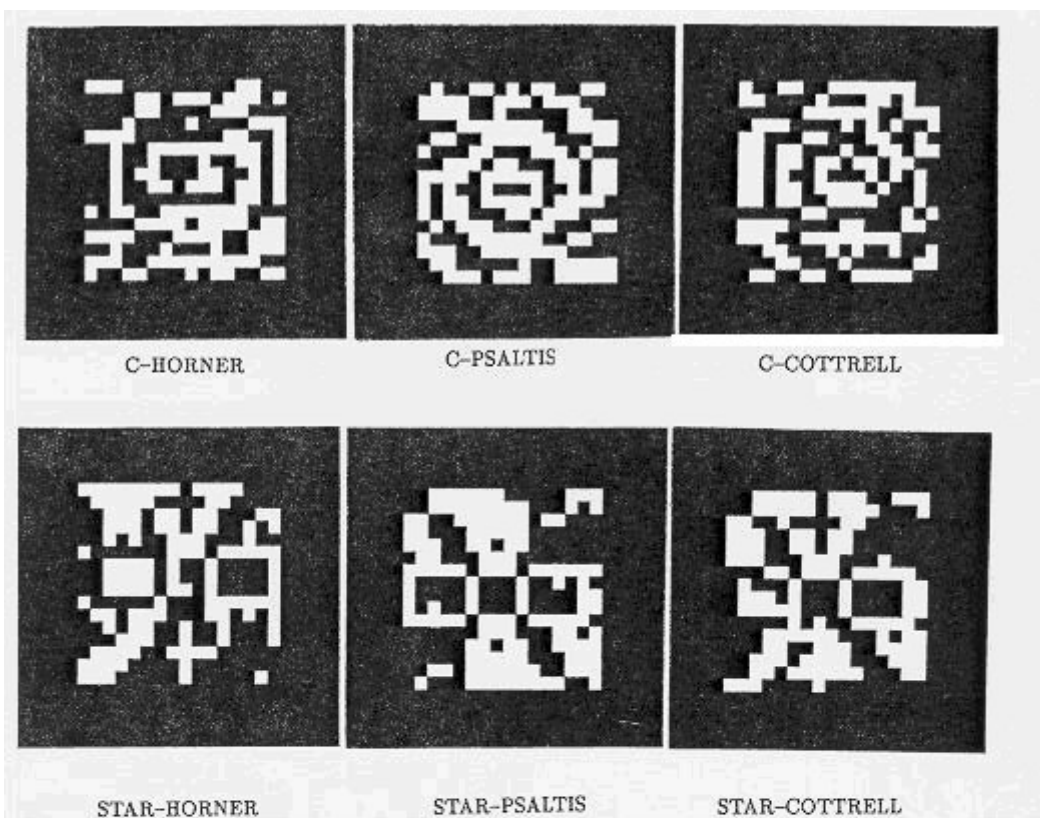


Figure 8.20: Filters for Target Objects 'C' and 'STAR'.

Figure 8.20: Filters for Target Objects 'C' and 'STAR'.

4.3 The Effect of Sample Number.

With the large variety of pixellated SLMs available, coupled with the free choice of f-number used in the optical processor, one may arrive at a very large number of samples being taken over each mirror if one samples at the PSR determined interval as described in chapter 7. This has important consequences for the combined technique which are now spelled out in detail.

One must recall a result of the 'central limit theorem', which states that if a large population has mean μ_p and standard deviation σ_p then the mean of a set of sample populations of size n is follows a Gaussian distribution with mean μ_p and standard deviation σ_s given by

$$\sigma_p$$

$$\sigma_s = \frac{\overline{\quad}}{\sqrt{n}} \quad (18)$$

One can imagine performing a very large DFT, say 1024×1024 , the statistics of which may be taken to very closely approximate those of the population referred to above, should they be required explicitly. It has been conjectured in this chapter that the phases Φ_{ij} follow an almost uniform distribution on the range $-\pi$ to $+\pi$, so that the population mean of the phase information is expected to be almost zero⁷. This has important consequences which bear directly on the filter creation process as described above.

1. The mean phases of each mirror are Gaussianly distributed about zero with a standard deviation of $[(\sigma_p)/(\sqrt{n})]$ where n denotes the number of pixels in each mirror.
2. As the number of DFT pixels n chosen to represent the spectrum over each mirror increases, the mean phase of the mirror approaches zero. This is equivalent to saying that the percentage of data Φ_{ij} lying on either side of the initial binarisation line approaches the same value of 50%, so that in the approximation of equation 8.9 the resulting distribution of the characteristic phases Φ_c becomes more tightly distributed about $[(\pi)/2]$. In this project, the distribution about $[(\pi)/2]$ is tight enough that nowhere does the Cottrell binarisation line intersect it, and so only the Psaltis threshold line, with $\beta = [(\pi)/2]$ can bisect the distribution to form a final filter with distinguishable mirror phases. This is illustrated in figure 8.21.

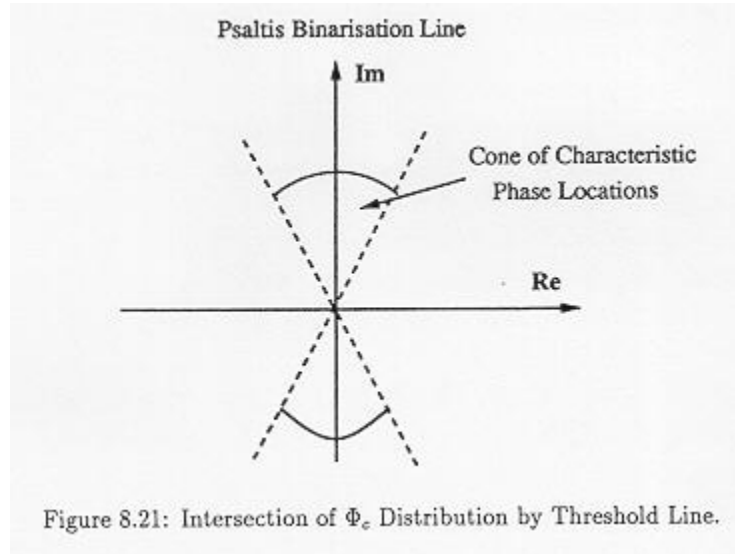


Figure 8.21: Intersection of Φ_c Distribution by Threshold Line.

3. Mirrors represented by very small DFT sub-arrays, however, have a very much wider distribution of Φ_c (by equation 8.10) due to the wider difference between n_A and n_B . Consequently, after initial binarisation and intensity averaging have been performed, the range of threshold angles which will intersect the distribution of Φ_c is much larger. The minimum array size n_{\min} for which the Horner binarisation line ($\beta = 0$) can still intersect the distribution will depend on σ_p by equation 8.18. SLMs of larger array size than the 16×16 used in this project will, for the same size of Fourier Transform (e.g. 256×256) have a reduced density of data pixels and filters fabricated with a wider range of final binarisation lines than used in this project may be investigated.

5 Chapter Summary

The low space-bandwidth product of the 16×16 phase modulating SLM demands that appropriate effort be made to devise quality auto-correlation algorithms for its appraisal as an binary, phase-only optical correlator. In this chapter several phase binarisation algorithms commonly used in correlator systems have been introduced and

briefly analysed as to their dependence on target object symmetry, for instance. A general framework suitable for the discussion of any filter computation procedure has been introduced, and the comparison of two such techniques formed the basis of the experimental work of this chapter.

The 'Combined Technique' devised in this project has been shown in computer simulations to produce slightly better auto-correlations than the technique of coherent summation, although there is little to choose between the two experimentally. Although a complete analysis of the CA technique has been performed, it is not the intention of this thesis to propose that this replace the procedure of coherent summation in auto-correlation work. Indeed, the CA technique has been the result of allowing complete freedom of choice in the overall framework of filter computation and it is remarkable that such an effective algorithm should have arisen from this.

In summary, it has been found that the Psaltis final binarisation algorithm applied to coherently summed spectral data over each mirror produces the best auto-correlation results (as judged by peak sharpness and peak energy) for the coherent summation filters. This is in agreement with the results of Downie et al [68] described in section 8.1.8. It is also found that if one initially binarises the spectral phase data according to the Psaltis algorithm, performs an intensity weighted average of these binarised phases to obtain a characteristic phase Φ_c for each mirror, and finally binarises Φ_c again according to Psaltis, one obtains a filter at least as good, if not better, as that obtained by coherent summation. The auto-correlations depicted in figures 8.7 and 8.10 show the results of the two best filter computation algorithms.

Footnotes:

¹ In the summer of 1991 the experimental results of this chapter were presented at the annual conference of the Society of Photo-Instrumentation Engineers, San Diego, California. The corresponding paper was based on an unpublished paper by Ranshaw but all experimental procedures and results are due to the author of this thesis. The paper, entitled 'Optical correlation using a phase-only liquid crystal over silicon spatial light modulator', may be found towards the end of this thesis.

² A detailed analysis of the *combined* algorithm technique follows the experimental results of this chapter.

³ Filters are termed equivalent if they share the same binarisation algorithm, whether it be used as an initial stage (intensity weighted Φ_c) or final stage (coherent summation).

⁴ The replication chosen was the first one off-axis to avoid the glare from the front-face reflection of the SLM which produced a constant intensity inverted image of the object.

⁵ The 'B' object is an exception to this however.

⁶ A symmetric object function will, however, have an entirely REAL Fourier Transform and as such the phases Φ_{ij} over any particular mirror must be either 0 or π ($\cos(\Phi_{ij}) = \pm 1$ when Φ_{ij} is 0 or π .) However, the Fourier synthesis of an arbitrary input function will generally require a much wider distribution of spatial frequency offsets (phase) than this and, with the exception of symmetric functions and several physically unlikely target object functions, may be approximated as a uniformly distributed random variable on the range $-\pi, +\pi$.

⁷ This will not be true for objects exhibiting a high degree of symmetry however.